PROCEEDINGS OF SCIENCE

Aggregating complementary instrument datasets with needlets for SZ component separation

PoS(Big3)030

Mathieu Remazeilles[*][†]
Institut d'Astrophysique Spatiale, Université Paris-Sud 11 & CNRS (UMR 8617), Orsay, France
E-mail: mathieu.remazeilles@ias.u-psud.fr

We propose to aggregate datasets from complementary CMB experiments with the intent of optimizing component separation and foreground cleaning for the reconstruction of the Sunyaev-Zeldovich (SZ) effect. In this purpose, we perform component separation on a wavelet frame by using a needlet ILC (internal linear combination) filter, showing that needlets are a flexible wavelet family to adapt the needlet localization of the filter to the beam of each experiment. To illustrate the approach, we perform SZ reconstruction with a needlet ILC exploiting jointly Planck-like and ACT-like instrument data. For each needlet scale, we perform an ILC combination of some specific channels, either from one instrument or from both instruments, selected for their relevance to the angular scale considered. Such a multiscale and multi-instrument component separation benefits simultaneously from a large number of channels to minimize the foreground contamination and from high-resolution channels to extract the SZ signal from compact galaxy clusters.

Big Bang, Big Data, Big Computers
September 19-21, 2012
Laboratoire Astroparticule et Cosmologie, 10 rue A. Domon et L. Duquet, 75205 Paris 13, France

---

[*] Speaker.

[†] Based on the work done in collaboration with Nabila Aghanim and Marian Douspis, reported in [1].

1. Introduction

Primordial CMB photons that scatter off the hot gas of electrons in galaxy clusters undergo a spectral distortion in the direction of the clusters that can be detected by the current CMB experiments [2, 3, 4]. This spectral distortion, known as thermal Sunyaev-Zeldovich (SZ) effect [5], has the advantageous property of being independent of the redshift, thus making the detection of the SZ effect a powerful and unique tool to probe compact galaxy clusters at any high redshift. The reconstruction of galaxy cluster profiles through thermal SZ (TSZ) effect is an exciting challenge also because the SZ profile, which is proportional to the density of electrons, is a formidable probe of the baryon physics in the cluster outskirts, beyond the radius of virialization, where X-ray measurements fail to reconstruct the thermal pressure profile.

The current sky observation in microwave frequency channels by different CMB experiments actually is a mixture of various emissions: CMB emission from the last scattering surface, SZ effect from galaxy clusters, foreground emission from the Galactic insterstellar medium, cosmic infrared background (CIB) emission from the galaxies, compact emission from extragalactic radio sources. Each of these components has a distinctive spectral signature, a distinctive spatial distribution on the sky, and a distinctive distribution on the angular scales. The separation of the different components and their individual reconstruction can thus be achieved by a multifrequency coherent analysis taking advantage of the distinct spectral signatures of the components. A review of various component separation methods can be found in [6] and the references therein. One of them, the ILC (Internal Linear Combination), benefits from the knowledge of the SZ frequency scaling as the only prior assumption, to reconstruct the SZ signal while minimizing the variance of the foreground sky contamination, without requiring any parametrization for the unknown foregrounds. In practice, the main limitation in reconstructing the SZ emission from compact clusters comes both from the achievable resolution of the instrument and from the level of contamination by the other sky emissions and the instrumental noise. While the first problem depends on the achievable beam of the instrument, the second one relies more on the number of available frequency channels that can be exploited by the component separation method as additional information to minimize the foreground contamination.

No single experiment provides the best SZ measurement. Space-borne instruments, like Planck, observe the whole sky with many frequency channels thus enabling component separation methods to have substantial information for removing the sky contamination, but those instruments are limited in resolution, which reduces the ability of the filters to recover the SZ signal from compact clusters. Conversely, ground-based instruments, like the Atacama Cosmology Telescope (ACT), benefit from higher-resolution beams to recover the SZ signal from compact clusters. However, because of the atmosphere, ground-based instruments suffer from a few number of frequency channels for observing the sky, therefore limiting the ability of component separation methods to minimize the foreground contamination. As long as a “super instrument”, both with many channels and high-resolution, for component separation is not available , we propose to “construct it” by aggregating complementary datasets from multiple available experiments.

The aggregation of heterogeneous instrument datasets has been first applied in [7], where the authors combined many CMB maps produced by different CMB experiments in order to optimize the estimation of the CMB power spectrum. Here we are interested in aggregating multiple instrument datasets for component separation purposes and foreground removal. Our purpose is both to increase the number of exploited channels in order to minimize the foreground contamination and to add high-resolution channels for extracting the SZ signal from compact clusters. We highlight how needlet decomposition can be used as a flexible wavelet sampling to aggregate multiple instrument datasets in a component separation process, by adapting the needlet scale windows to the individual beams of each instrument. To support our approach, we perform thermal SZ reconstruction by applying a needlet ILC filter [8] on three simulated datasets: a Planck-like dataset, a ACT-like dataset, and a Planck-like/ACT-like aggregated dataset. For the first time, we provide forecasts for a SZ effect reconstruction exploiting multiple instrument datasets jointly. The results exposed in this communication are presented in greater detail in [1].

2. Aggregating many experiments with needlet ILC

Pixel-based component separation methods, like the ILC filter implemented in pixel space by the WMAP collaboration to extract the CMB map [9], suffer from nonlocality in harmonic (or Fourier) space because of the incertainty principle, so that they need to combine maps probing the same angular scales. Consequently, component separation in pixel space must be performed by a weighted combination of the same set of channel maps, fixed for all the angular scales considered. Say otherwise, pixel-based methods require either to degrade all the channel maps to a common resolution, which is compelled to be the lowest resolution of the set of maps, or to reject the channels that have a higher resolution. As being either resolution-limited or channel-limited, pixel-based component separation methods are not suited to combine channel maps from multiple experiments with various resolutions.

Conversely, component separation methods that are implemented in Fourier space suffer from nonlocality in pixel space because of the same incertainty principle. Therefore, methods inplemented in Fourier space can not easily handle data from a partial sky coverage, such as the data of ground-based CMB experiments. In that sense, Fourier space component separation methods are not suitable for aggregating heterogeneous instrument datasets.

For the purpose of aggregating multiple instrument datasets with various resolutions in a component separation process, our best compromise is to perform a wavelet-based component separation by decomposing the filter on a wavelet frame. The properties of wavelet localization, both in scale and in space, have proved robust to adapt component separation methods to local conditions of contamination (galactic contamination on large scales and low galactic latitude, instrumental noise on small scales). Here, wavelet localization is shown to be also robust for component separation filters to combine aggregated datasets from multiple instruments with various specifications.

In particular, we propose to develop a needlet ILC (NILC) filtering on patch to reconstruct the SZ signal in specific regions of the sky by exploiting aggregated datasets from different experiments. The formulation of the needlets in CMB data analysis can be found in [10]. Needlets are a particular wavelet family that does not require dyadic sampling. Therefore, they are flexible enough to adapt the localization in Fourier space, so that the needlet windows can be defined for matching the individual beams of each instrument. As a general example, let us consider two experiments noted EXP1 and EXP2, the former having a lower resolution θ_1 than the latter having a beam $\theta_2 < \theta_1$, but a larger number of frequency channels $N_1 > N_2$. For the sake of simplicity

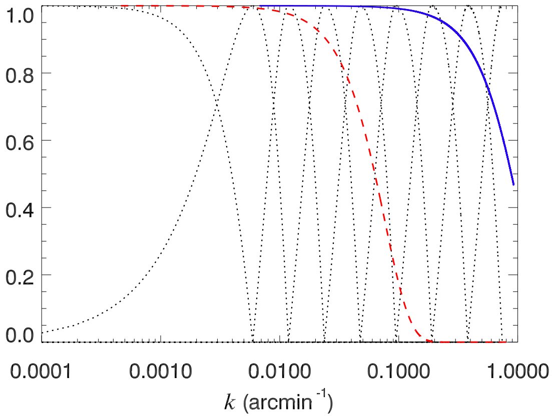

Figure 1: Illustration of needlet scales versus beams. In this plot we assume $N_1 = 5$ and $N_2 = 4$. The beam of EXP1 channels (thick dashed red) and the beam of EXP2 channels (thick solid blue) are overplotted on the needlet bands (thin dotted black). For each needlet band an ILC estimate is computed: in the first five bands the NILC processing combine EXP1 and EXP2 channels whereas in the last four bands only EXP2 channels are exploited by NILC.

we assume that the N_1 (resp. N_2) channel-maps of EXP1 (resp. EXP2) have the same resolution θ_1 (resp. θ_2). We may define $N_1 + N_2$ needlet bands $h_k^{(j)}$ in the Fourier domain, indexed by j, such that, over the useful range of spatial frequency k, we have

$$\sum_j \left[h_k^{(j)}\right]^2 = 1, \tag{2.1}$$

and in such a way that the beam of EXP1, θ_1, can not probe the scales $k > k_{\max}^{(N_1)}$, where $k_{\max}^{(N_1)}$ is the highest Fourier mode probed by the N_1^{th} needlet band $h_k^{(N_1)}$ (see Fig. 1). The $(N_1 + N_2)$ available channel maps (or patches) can be written in a vector form as

$$\mathbf{x}(p) \;=\; \mathbf{a}s(p) + \mathbf{n}(p) \tag{2.2}$$

where p denotes the pixel. Here the vector $\mathbf{x}(p)$ collects the $(N_1 + N_2)$ frequency maps observed by EXP1 and EXP2, $s(p)$ is the unknown thermal SZ template map that we would like to reconstruct, and $\mathbf{a}$ is the known frequency scaling vector of the SZ effect. All the other sky emissions (CMB, foregrounds) and the noise are collected into a single nuisance term $\mathbf{n}(p)$. In the following NILC component separation is performed on patches of the sky smaller than 100 square degrees so that flat-sky approximation is adopted and fast Fourier transforms (FFT) are used in place of spherical harmonic transforms. Such a patch-NILC method has the advantage of offering a fast algorithm suited for reconstructing the SZ signal on small regions of the sky centred on particular clusters.

Maps of needlet coefficients $x^{(j)}(p)$ *at a given scale* (j) are obtained, for the observed maps $\mathbf{x}(p)$, by inverse FFT of the associated map Fourier coefficients $\mathbf{x}_k$ filtered by the spectral windows $h_k^{(j)}$:

$$\mathbf{x}^{(j)}(p) = \sum_{k_1=0}^{N_k-1} \sum_{k_2=0}^{N_k-1} h_k^{(j)} \mathbf{x}_k \exp\left[i2\pi\left(\frac{k_1}{N_k}p_1 + \frac{k_2}{N_k}p_2\right)\right] \tag{2.3}$$

where $p=(p_1,p_2)$, $k=\sqrt{k_1^2+k_2^2}$ and N_k is the number of resolution elements on each side of the two-dimensional FFT patch considered. The ILC estimate of the SZ map is a weighted linear combination of the observed maps of minimum variance under the constraint of offering unit response to the SZ component. At the needlet scale (j), straightforward algebra using Lagrange multiplier yields to the following NILC estimate:

$$\widehat{s}^{(j)}(p)=\mathbf{w}^T\,\mathbf{x}^{(j)}(p)=\frac{\mathbf{a}^T\,(\widehat{\mathbf{R}}^{(j)}(p))^{-1}}{\mathbf{a}^T\,(\widehat{\mathbf{R}}^{(j)}(p))^{-1}\mathbf{a}}\,\mathbf{x}^{(j)}(p), \tag{2.4}$$

where $\widehat{\mathbf{R}}^{(j)}$ is the local covariance matrix of the needlet coefficients of the observations:

$$\widehat{\mathbf{R}}_{ab}^{(j)}(p)=\frac{1}{N_{\rm p}}\sum_{p'\in\mathscr{D}_p}x_a^{(j)}(p')x_b^{(j)}(p'). \tag{2.5}$$

The pixel domain $\mathscr{D}_p$, on which the local covariance is computed, is defined from the smoothing of the product map $x_a^{(j)}(p)x_b^{(j)}(p)$ with a symmetric Gaussian window in pixel space.

The intent here is to benefit both from the maximum number of channels N_1+N_2 and from the highest resolution θ_2 when performing NILC component separation, both conditions being required to guarantee a reconstructed TSZ signal with the lowest sky residuals and with the highest resolution. Therefore, ILC filtering is performed at each needlet scale (j) by combining the channel-maps whose resolution is compatible with the needlet band $h_k^{(j)}$ considered. Typically, in the bands (j), where $1\leq j\leq N_1$, the ILC TSZ output $\widehat{s}^{(j)}(p)$ results from the combination of the N_1+N_2 maps of both EXP1 and EXP2. Next, in the following bands (j) where $N_1+1\leq j\leq N_2$, the ILC combination is performed on the N_2 higher resolution maps of EXP2 only, the maps of EXP1 having no information at the scales covered by the N_2 latest bands to be taken into account in the ILC combination. Formally, for all $j\leq N_1$ the ILC estimate is computed from the combination of both the EXP1 dataset and the EXP2 dataset

$$\begin{aligned}\widehat{s}^{(j)}(p) \;=\; & w_1^{(j)}x_{1;\,\mathrm{EXP1}}^{(j)}(p)+\ldots+w_{N_1}^{(j)}x_{N_1;\,\mathrm{EXP1}}^{(j)}(p)\\ & +w_{N_1+1}^{(j)}x_{N_1+1;\,\mathrm{EXP2}}^{(j)}(p)+\ldots+w_{N_1+N_2}^{(j)}x_{N_1+N_2;\,\mathrm{EXP2}}^{(j)}(p),\end{aligned} \tag{2.6}$$

while for all $j>N_1$ the ILC is computed from the combination of the EXP2 dataset only

$$\widehat{s}^{(j)}(p) \;=\; w_{N_1+1}^{(j)}x_{N_1+1;\,\mathrm{EXP2}}^{(j)}(p)+\ldots+w_{N_1+N_2}^{(j)}x_{N_1+N_2;\,\mathrm{EXP2}}^{(j)}(p). \tag{2.7}$$

The synthesis of the needlet SZ estimates is achieved by the following scheme

$$\widehat{s}^{(j)}(p)\xrightarrow{\mathrm{FFT}}h_k^{(j)}\widehat{s}_k\xrightarrow{\times}\left(h_k^{(j)}\right)^2\widehat{s}_k\xrightarrow{\mathrm{FFT}^{-1}}\widehat{z}^{(j)}(p), \tag{2.8}$$

where the reconstructed “SZ maps per scale” $\widehat{z}^{(j)}(p)$ are then coadded to provide the complete SZ estimate

$$\widehat{s}(p)=\sum_j\widehat{z}^{(j)}(p). \tag{2.9}$$

Equation (2.1) on the needlet windows guarantees the conservation of the SZ power in the processing Eqs. (2.8) and (2.9).

Planck-like	30 GHz	90 GHz	148 GHz	219 GHz	350 GHz	545 GHz
θ [arcmin]	32.65	9.88	7.18	4.71	4.5	4.72
σ_N(4 surveys) [μK $\cdot$ arcmin]	210	57	30	44	173	2485

ACT-like	148 GHz	219 GHz	277 GHz
θ [arcmin]	1.4	1.0	0.9
σ_N [μK $\cdot$ arcmin]	30	45	60

Table 1: Specifications of both datasets constructed from the sky simulation of [11]. Beams and noise RMS for Planck maps refer to 4 full-sky surveys (28 months). ACT values refer to the 2008 ACT Southern survey.

Needlet ILC thus appears as a multiscale, or multiresolution, tool to aggregate multiple experiments with various specifications for component separation: on the larger angular scales NILC is used for removing the Galactic foreground contamination by combining a large number of channels (both EXP1 and EXP2), while on the smaller angular scales NILC is recovering the SZ effect at higher resolution by combining the high-resolution channels of EXP2 only.

3. Thermal SZ reconstruction from combined Planck-like/ACT-like data

3.1 Maps and spectra

We consider the high-resolution simulation of the microwave sky developed in [11] to construct both a Planck-like experiment and a ACT-like experiment. The simulation of the sky emission includes the CMB emission, the SZ effect, the galactic foreground emission, and emission from radio and infrared galaxies. The specifications of the simulated instruments (beams, noise RMS, and frequency channels) are collected in Tab. 1. The Planck-like instrument is a many-channel experiment with limited resolution (about 5 arcmin), whereas the ACT-like instrument is a few-channel experiment with higher resolution (about 1 arcmin). Figure 2 shows some of the inputs of the simulation (thermal SZ, thermal dust, Planck-like 90GHz observation, and ACT-like 277GHz observation) on a $7^\circ \times 7^\circ$ patch of the sky centred on the extended cluster 1 of Tab. 2.

The reconstruction of the thermal SZ effect is illustrated on two distinct patches of the sky centered on the selected clusters given in Tab. 2 (an extended cluster with $\theta_{200} = 40.7$ arcmin and a compact one with $\theta_{200} = 3$ arcmin)[1]. We generalise the analysis to a sample of selected clusters in Sect. 3.2.

In Fig. 3 we perform NILC filtering on three sets of data to reconstruct the TSZ signal: on the single Planck-like dataset, on the single ACT-like dataset, and on the joint Planck-like/ACT-like dataset. The top panels of Fig. 3 show the reconstruction of the TSZ effect from the extended cluster 1 of Tab. 2. The top left panel is the input signal at 10 arcmin resolution and the successive NILC reconstructions from the single Planck-like, single ACT-like, and joint Planck/ACT datasets are respectively shown on the second top panel, the third top panel, and the fourth top panel (from left

---

[1] Here we define $\theta_{200} = R_{200}/D_A$ where R_{200} is the radius in which the total density contrast of the cluster is $\delta = 200$, as compared to the critical density of the Universe at the cluster redshift, and D_A is the angular diameter distance to the cluster.

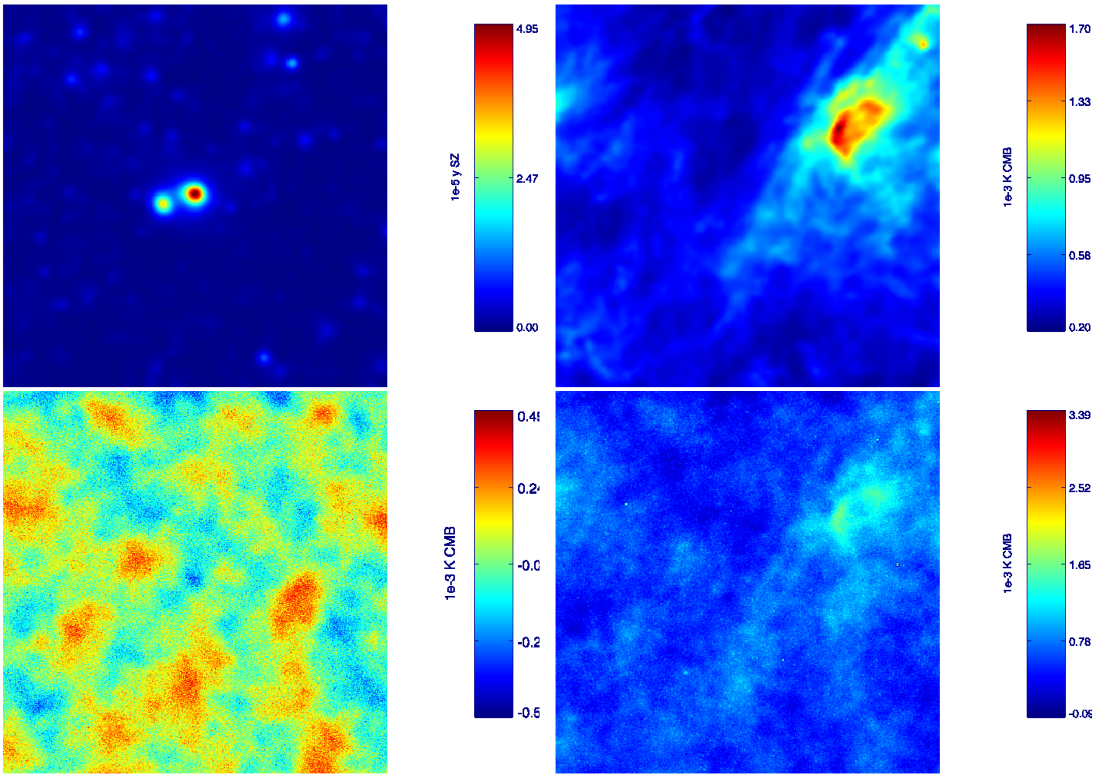

Figure 2: A 7° × 7° patch of the simulated sky centered on the selected cluster 1 of Tab. 2. On the top panels: input thermal SZ smoothed to 10 arcmin resolution (left) and Galactic dust at 277GHz (right). On the bottom panels: Planck-like 90GHz channel-map (left) and ACT-like 277GHz channel-map (right).

to right). The reconstruction exploiting data from the single ACT-like instrument (third top panel) shows more contamination by galactic foregrounds than the reconstruction exploiting Planck-like data (second top panel), some residual dust being visible on the top right corner of the third top panel (to be compared to the input dust map in Fig. 2). This is expected because of the few number of channels that are exploited by the NILC filter when using the single ACT-like dataset. Exploiting the Planck-like dataset enables NILC to have more information, through a larger number of available channels, to remove foreground contamination. When applying NILC to the aggregated Planck-like/ACT-like dataset, the background noise (sky contamination and instrumental) is minimized even further than in single-instrument reconstructions because of the increased number of frequency channels combined by NILC. On the bottom panels of Fig. 3 we show the results of NILC filtering, at 3 arcmin resolution, on another patch of sky centred on the compact cluster 2 of Tab. 2. Such a compact cluster has a typical angular size smaller than the achievable Planck beam. In that case, the single Planck-like reconstruction (second bottom panel) fails in recovering the SZ signal from the compact cluster, because of the lack of resolution of the exploited channels, and the result is completely noisy. Conversely, the SZ signal can be recovered when exploiting the three high-resolution channels of the ACT-like instrument (third bottom panel). However, ACT-like reconstruction is still contaminated by foregrounds because of the lack of exploited channels. The best compromise is obtained by applying NILC on the joint Planck-like/ACT-like dataset (fourth

	z	R.A. [degree]	Dec. [degree]	M_{200} $[10^{14} M_{\odot}]$	R_{200} [Mpc]	θ_{200} [arcmin]	Y_{200} $[\text{arcmin}^2]$
cluster 1	0.04	39.6	15.8	7.3	1.82	40.7	0.0299
cluster 2	0.95	2.5	78.0	9.7	1.45	3.0	0.0007

Table 2: Two selected clusters from the SZ Halo catalog of the simulation in [11]. For each cluster, the table collects redshift, coordinates (R.A., Dec.), mass, radius, angular size, integrated Compton value within R_{200}.

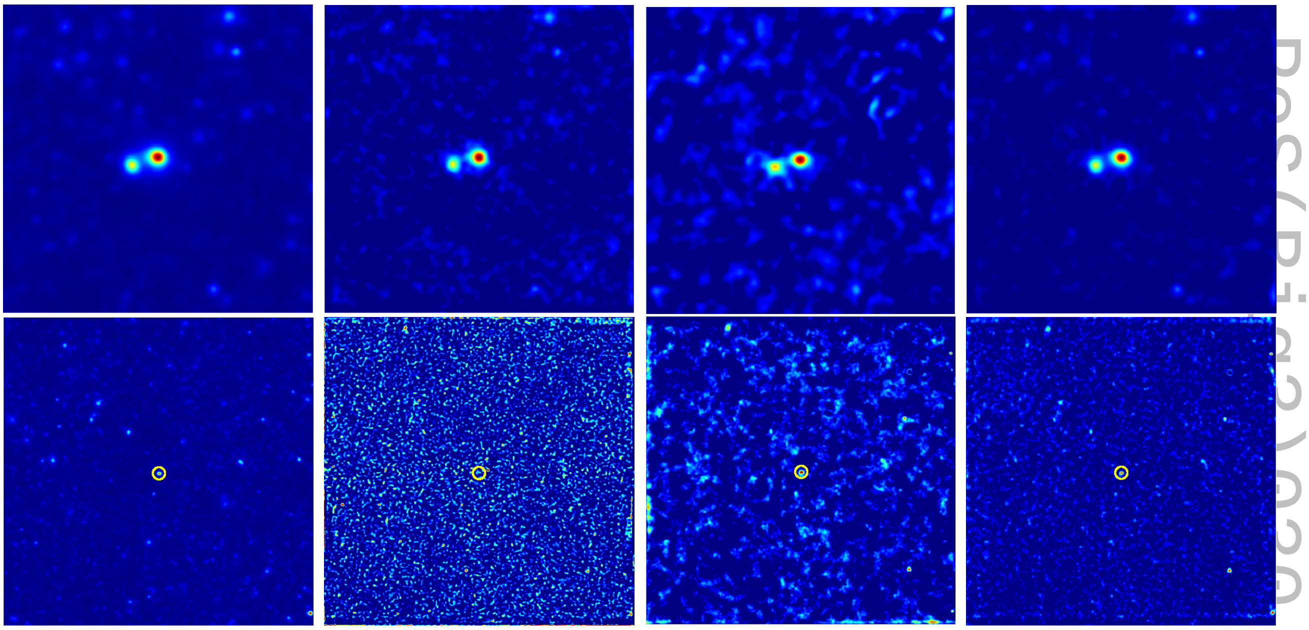

Figure 3: NILC reconstruction of the thermal SZ effect using different datasets. From left to right panels: input TSZ signal, NILC TSZ reconstruction from Planck-like channels only, NILC TSZ reconstruction from ACT-like channels only, NILC TSZ reconstruction from the combination of complementary data, i.e. both Planck-like and ACT-like channels. Top panels: reconstruction centred on cluster 1 of Tab. 2. Bottom panels: reconstruction centred on cluster 2 of Tab. 2.

bottom panel), where we simultaneously recover the SZ signal from the compact cluster, due to the combination of high-resolution ACT-like channels, and remove the background noise, due to the large number of exploited channels.

We also compute the power spectrum of the TSZ reconstruction for the extended cluster 1 of Tab. 2. On the top left panel of Fig. 4 we plot the TSZ power spectra for the various reconstructions presented on the top panels of Fig. 3, where the output resolution is 10 arcmin. We clearly see that the joint Planck/ACT power spectrum best recovers the input TSZ power spectrum. On the top right panel of Fig. 4, the same plot is shown in the case where the reconstruction has been performed at higher resolution: 3 arcmin for both single ACT-like and joint Planck/ACT reconstructions, and 5 arcmin for single Planck-like reconstruction, the beam of Planck-like channels being limited. In that case, the reconstruction is noisier. On the large scales $k < 0.1$ arcmin^{-1}, the Planck-like reconstruction recovers the TSZ power spectrum better than the ACT-like reconstruction, whereas

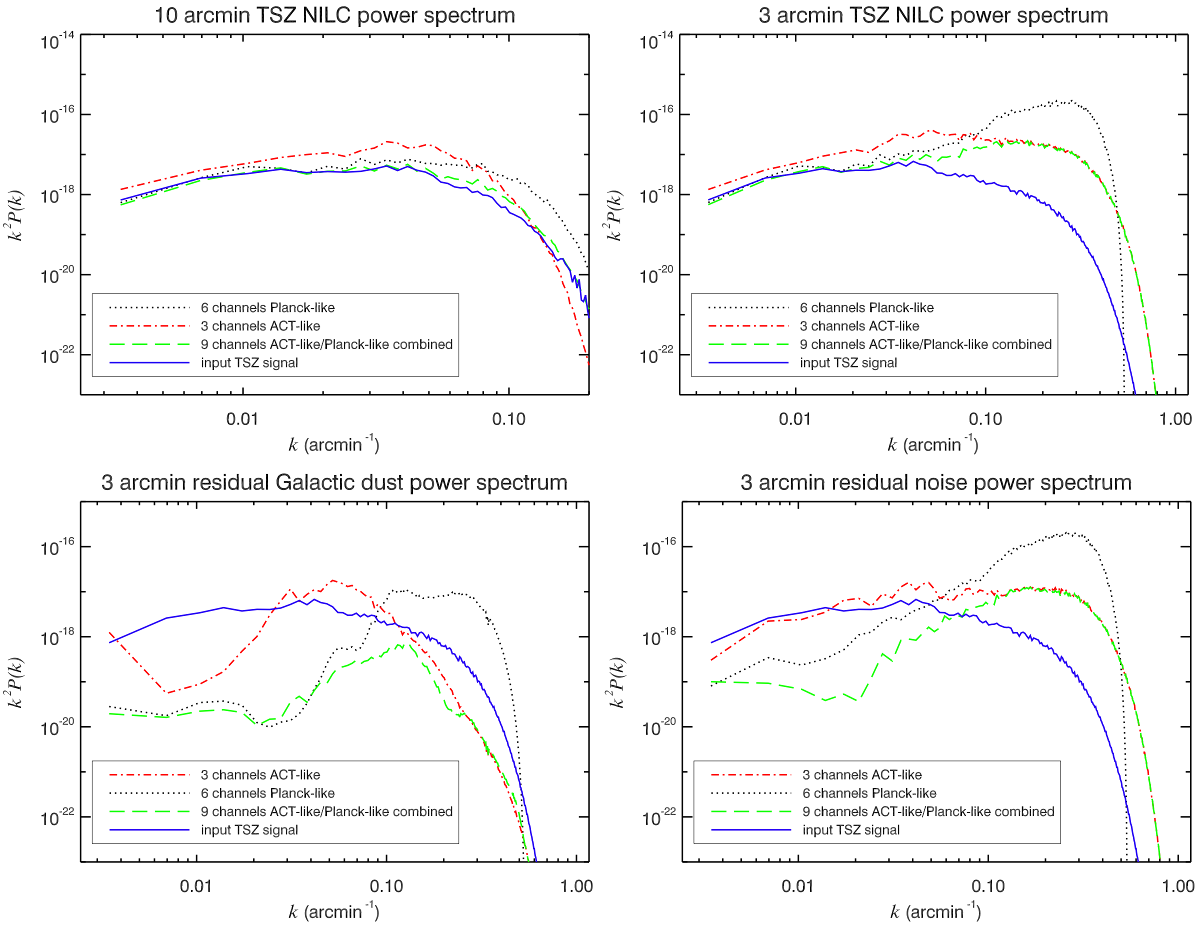

Figure 4: NILC thermal SZ power spectra from different datasets for 10 arcmin reconstruction (top left panel) and 3 arcmin reconstruction (top right panel) versus input power spectrum (selected cluster 1 of Tab. 2). At the smallest scales, the Planck-like TSZ spectrum is noisy compared to the ACT-like TSZ power spectrum and limited to the instrumental beam. The joint Planck-like/ACT-like TSZ spectrum matches very well the input thermal SZ spectrum at 10 arcmin resolution. Residual Galactic dust power spectra (bottom left panel) and residual instrumental noise power spectra (bottom right panel) for the 3 arcmin TSZ reconstruction are also plotted for comparison. At the largest scales, the TSZ spectrum reconstructed from Planck-like data is less contaminated by the residual Galactic dust than the TSZ power spectrum from ACT-like data because of the larger number of channels combined by ILC. The joint Planck-like/ACT-like reconstruction shows the best reduction of the residual dust power on all scales.

it is the opposite on small scales $k > 0.1$ arcmin^{-1}. The joint Planck/ACT power spectrum matches the Planck-like power spectrum on the large scales $k < 0.1$ arcmin^{-1} while matching the ACT-like power spectrum on the smaller scales $k > 0.1$ arcmin^{-1}, thus providing the best trade-off on all scales. By applying the ILC weights onto the input dust maps of the simulation, we can compute the residual dust contamination in the reconstructed TSZ power spectrum: on the bottom left panel of Fig. 4, the ACT-like reconstruction clearly shows more contamination by galactic dust than the Planck-like reconstruction on the large scales ($k < 0.1$ arcmin^{-1}). This is due to the few number of available channels when NILC is applied on the ACT-like instrument dataset. At smaller scales, the Planck-like reconstruction shows more galactic residuals because the ILC weights are requested for minimizing the instrumental noise which becomes the dominant contaminant here, as it can be also seen on the residual noise power spectrum plotted in the bottom right panel of Fig. 4. The reconstruction of the TSZ power spectrum from the joint exploitation of Planck-like and ACT-like datasets reduces further the power of residual dust on all scales (bottom left panel of Fig. 4), by matching the Planck-like reconstruction on large scales $k > 0.1$ arcmin^{-1} and the ACT-like reconstruction on smaller scales. In that case where both instrument datasets are aggregated, galactic dust residuals are two orders of magnitude below the TSZ signal. The level of instrumental noise residuals is also reduced on all scales by the joint reconstruction, unlike single-instrument reconstructions (bottom right panel of Fig. 4).

3.2 SZ profiles: statistical analysis on a sample of clusters

We now investigate the reconstruction of the SZ profile of clusters by considering a sample of 90 galaxy clusters selected from the catalog in [11]. The selected sample consists in three sub-samples of 30 clusters each: a sub-sample of 30 extended clusters with 15 arcmin $< \theta_{200} <$ 40 arcmin, a sub-sample of 30 "typical" clusters with $\theta_{200} \sim 5$ arcmin, and a sub-sample of 30 compact clusters with $\theta_{200} \sim 3$ arcmin. Their different locations on the sky allow us to explore different levels of sky background. We perform NILC on $7^\circ \times 7^\circ$ patches of the sky centred on each cluster of the sample by exploiting either single Planck-like channel observations, or single ACT-like channel observations, or joint Planck-like/ACT-like channel observations. The results on the mean TSZ profile are shown in Fig. 5.

On the sample of extended clusters (top panels of Fig. 5), the reconstruction of the SZ profile is reliable for the three sets of data (Planck-like, ACT-like, and joint datasets) with the ACT-like reconstruction slightly more contaminated by the sky background on the tail of the profile. This is confirmed when we look at the contamination by Galactic dust in the reconstructed TSZ profile in Fig. 6: residual dust has larger amplitude for the ACT-like reconstruction. The exploitation of a larger number of channels in the Planck-like and joint Planck/ACT reconstructions reduces the amplitude of the foreground residuals in the TSZ profile. Conversely, on the middle left and bottom left panels of Fig. 5, we see that a component separation applied on the single Planck-like dataset completely fails in reconstructing the SZ profile from compact galaxy clusters. When we are interested in reconstructing the SZ profile from compact clusters with $\theta_{200} < 5$ arcmin (middle panels and bottom panels of Fig. 5) we can take advantage of the high-resolution ACT-like channels to go beyond the limited beam of the Planck-like instrument.

To quantitatively assess the performance of the reconstruction, we can compute the mean squared error (MSE) measuring the trade-off between the bias and the variance of the profile reconstruction:

$$\mathrm{MSE} = \sum_{\mathrm{ring}\ i} \left[\left(\overline{Y}_i - \overline{Y}_i^{(\mathrm{in})} \right)^2 + \overline{\sigma}_i^2 \right], \tag{3.1}$$

where $\overline{Y}_i = \frac{1}{n}\sum_{j=1}^{n} \widehat{Y}_i^j$, $\overline{Y}_i^{(\mathrm{in})} = \frac{1}{n}\sum_{j=1}^{n} Y_i^{(\mathrm{in})j}$, and $\overline{\sigma}_i^2 = \frac{1}{n^2}\sum_{j=1}^{n} \left(\sigma_i^j\right)^2$ are quantities averaged on the sample considered. Here n is the size of the sample and the quantities indexed by j refer to one cluster of the sample, i.e. $\widehat{Y}^j$ is the reconstructed SZ profile from the cluster j, $Y^{(\mathrm{in})j}$ is the input

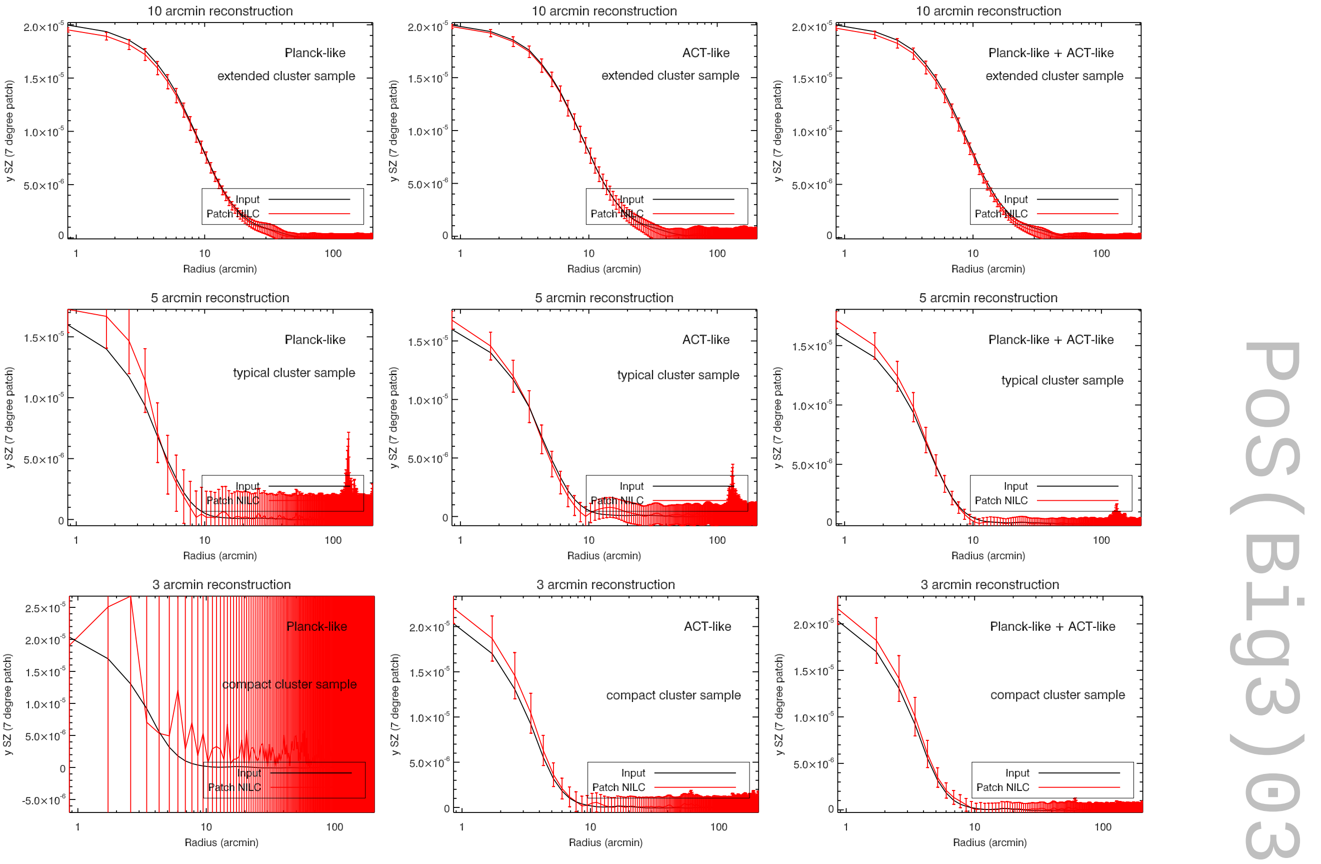

Figure 5: Cluster mean profiles for 7° × 7° patches of the sky. From left to right: reconstructed using Planck-like channels, reconstructed using ACT-like channels, reconstructed using jointly Planck-like/ACT-like channels. From top to bottom: sample of 30 extended clusters with 15 arcmin $< \theta_{200} <$ 40 arcmin, sample of 30 "typical" clusters with $\theta_{200} \sim 5$ arcmin, sample of 30 compact clusters with $\theta_{200} \sim 3$ arcmin.

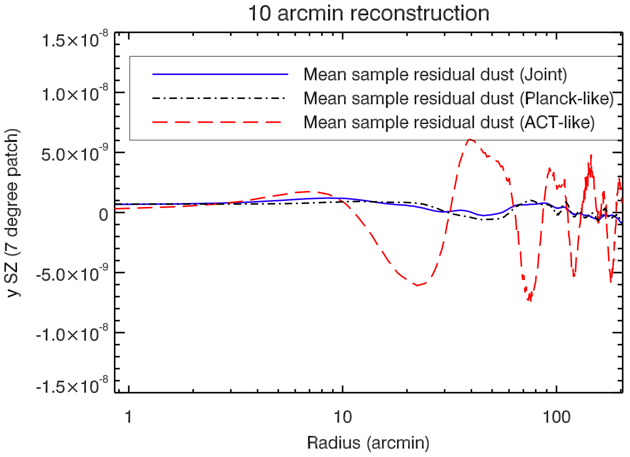

Figure 6: Residual dust mean profile (extended cluster sample). Planck-like (dot-dashed black), ACT-like (long dashed red), Planck-like/ACT-like combined (solid blue).

MSE (extended)	Planck-like	ACT-like	Joint
	3.95e–11	1.23e–10	3.35e–11
MSE (“typical”)	Planck-like	ACT-like	Joint
	1.27e–9	3.74e–10	8.12e–11
MSE (compact)	Planck-like	ACT-like	Joint
	6.52e–7	3.65e–10	1.45e–10

Table 3: Performance of the mean sample profile reconstruction measured by the criterion Eq. (3.1).

SZ profile from the same cluster, and σ_i^j is the standard deviation (error bar) on the reconstructed profile j for a ring i of N_p pixels:

$$\sigma_i^j = \sqrt{\frac{1}{N_\mathrm{p}-1}\sum_{p\,\in\,\mathrm{ring}\;i}\left(\widehat{y}^j(p)-\widehat{Y}_i^j\right)^2}, \tag{3.2}$$

where $\widehat{y}^j(p)$ is the NILC estimate of the SZ signal on the patch centred on the cluster j. In Tab. 3 we have listed the results for the three samples of clusters (extended, ”typical”, and compact) and for the three sets of exploited data (Planck-like, ACT-like, and joint Planck-like/ACT-like). The results on the extended cluster sample show that the reconstruction of the TSZ profile is achieved with almost similar accuracy for the three datasets, the ACT-like reconstruction being slightly less robust in removing galactic foreground contamination due to the lack of exploited channels. Conversely, Tab. 3 shows that NILC applied on the single Planck-like channels completely fails in reconstructing the SZ profile from more compact clusters ($\theta_{200} < 5$ arcmin) due to the lack of resolution of the Planck-like channels compared to ACT-like. For compact clusters, the joint Planck-like/ACT-like NILC significantly improves the reconstruction of the TSZ profile by two orders of magnitude. In any case the joint exploitation of both Planck-like and ACT-like observations by NILC provides the most accurate reconstruction of the TSZ profile, both in terms of resolution and in terms of foreground cleaning.

The SZ profile of galaxy clusters is a formidable candle to investigatt the baryon physics beyond the radius of virialization in the intracluster medium, where X-ray measurements have no information. The reconstruction of the SZ profile from galaxy clusters therefore is an exciting challenge in cosmology. We have presented the advantages of exploiting joint datasets from multiple experiments to reconstruct the SZ profile. First results from the data analysis of single CMB experiments have been recently provided [2, 3, 4]. Both in ACT [3] and SPT [2] results, a matched filtering approach has been implemented for reconstructing SZ profiles. Even if the matched filtering (e.g [12]) is an effective way of reconstructing the SZ profile when few frequency channels are available, it relies on a prior assumption on the cluster profile, which may appear controversial when we are interested in recovering SZ profiles. On the one hand, the needlet ILC on patch developed in this work is able to aggregate data from multiple CMB experiments. On the other hand, it is a blind approach that does not suffer from any prior to reconstruct the SZ profile.

References

[1] Remazeilles M., Aghanim N. and Douspis M., arXiv:1207.4683 [astro-ph.CO]

[2] Plagge T. et al., ApJ, 716, 1118 (2010), arXiv:0911.2444 [astro-ph.CO]

[3] Sehgal N. et al., ApJ, 732, 44 (2011), arxiv:1010.1025 [astro-ph.CO]

[4] Planck Collaboration at al., (2012), arxiv:1205.3376 [astro-ph.CO]

[5] Sunyaev R. A. and Zeldovich Y. B., Comments on Astrophysics and Space Physics (1972)

[6] Leach S. M. et al., A&A, 491, 597 (2008), arXiv:0805.0269 [astro-ph]

[7] Faÿ G. et al., Phys. Rev. D, 78, 083013 (2008), arXiv:0807.1113 [astro-ph]

[8] Delabrouille J. et al., A&A, 493, 835 (2009), arXiv:0807.0773 [astro-ph]

[9] Bennett C. L. et al., ApJS, 148, 97 (2003), arXiv:astro-ph/0302208

[10] Marinucci D. et al., MNRAS, 383, 539 (2008), arXiv:0707.0844 [astro-ph]

[11] Sehgal N. et al., ApJ, 709, 920 (2010), arXiv:0908.0540 [astro-ph.CO]

[12] Melin J.-B., Bartlett J. G. and Delabrouille J., A&A, 459, 341 (2006), arXiv:astro-ph/0602424